

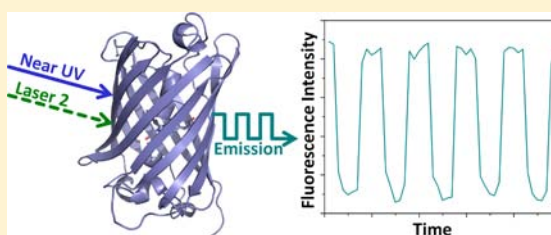
## Optically Modulatable Blue Fluorescent Proteins

Amy E. Jablonski,<sup>†,§</sup> Russell B. Vegh,<sup>†,§</sup> Jung-Cheng Hsiang,<sup>†,§</sup> Bettina Bommarius,<sup>‡,§</sup> Yen-Cheng Chen,<sup>†,§</sup> Kyril M. Solntsev,<sup>†</sup> Andreas S. Bommarius,<sup>‡,§</sup> Laren M. Tolbert,<sup>†</sup> and Robert M. Dickson<sup>\*,†,§</sup>

<sup>†</sup>School of Chemistry and Biochemistry, <sup>‡</sup>School of Chemical and Biomolecular Engineering, and <sup>§</sup>Petit Institute for Bioengineering and Bioscience, Georgia Institute of Technology, Atlanta, Georgia 30332-0400, United States

**S** Supporting Information

**ABSTRACT:** Blue fluorescent proteins (BFPs) offer visualization of protein location and behavior, but often suffer from high autofluorescent background and poor signal discrimination. Through dual-laser excitation of bright and photoinduced dark states, mutations to the residues surrounding the BFP chromophore enable long-wavelength optical modulation of BFP emission. Such dark state engineering enables violet-excited blue emission to be increased upon lower energy, green coillumination. Turning this green coillumination on and off at a specific frequency dynamically modulates collected blue fluorescence without generating additional background. Interpreted as transient photoconversion between neutral cis and anionic trans chromophoric forms, mutations tune photoisomerization and ground state tautomerizations to enable long-wavelength depopulation of the millisecond-lived, spectrally shifted dark states. Single mutations to the tyrosine-based blue fluorescent protein T203V/S205V exhibit enhanced modulation depth and varied frequency. Importantly, analogous single point mutations in the nonmodulatable BFP, mKalamal, creates a modulatable variant. Building modulatable BFPs offers opportunities for improved BFP signal discrimination vs background, greatly enhancing their utility.



### INTRODUCTION

Essential to a wide array of biological studies, fluorescent protein (FP) variants have been optimized for brightness, photoswitching, and maturation time, over a wide spectral range.<sup>1</sup> Enabling unparalleled glimpses into cellular structure and dynamics,<sup>2–6</sup> their facile, minimally perturbative labeling of multiple intracellular targets has cemented their role in cellular imaging. Thus, FPs are the preferred choice for biosensor development, protein–protein interaction visualization, and measurements of intracellular dynamics.<sup>7–10</sup> The 11-stranded  $\beta$ -barrel structure and chromogenic XYG peptide are common among essentially all GFP-like proteins.<sup>11</sup> Various color emitters are made by either extending the chromophore conjugation length or tuning the 3-D solvation shell, affecting cis–trans isomerization and chromophore protonation state.<sup>6,11</sup> Thus, the residues surrounding the chromophore are key to creating and optimizing new fluorescent protein properties and tailoring them to new applications.<sup>12–14</sup>

Cellular imaging is still confounded by major limitations involving signal discrimination vs both autofluorescence and other exogenous labels. Although one approach would be continued improvement of far-red fluorescent proteins,<sup>15–17</sup> blue fluorescent proteins (BFPs) are also essential in multilabel/multicolor imaging schemes.<sup>18,19</sup> Initial advances in improving BFP photostability and brightness were achieved by enforcing neutrality of the chromophore by swapping the chromophore tyrosine for either histidine or phenylalanine, thereby altering the  $\pi$ -electron structure.<sup>20,21</sup> A parallel path in BFP optimization resulted from mutating residues in close proximity to the original tyrosine-containing chromophore<sup>18,22</sup>

to better stabilize the neutral form in the ground state and to block wavelength-shifting excited-state proton transfer (ESPT). A series of 22 mutations along this path resulted in the monomeric, blue-emitting mKalamal<sup>18</sup> that exhibits 3.6- and 25-fold improved brightness and photostability, respectively, over the original enhanced BFP.<sup>18</sup> However, the significant autofluorescence generated under near-UV excitation still limits utility of even the brightest available BFPs.

Recently, novel dual-laser modulation and signal recovery schemes have enabled discrimination of designer fluorophore signals by suppressing obscuring background.<sup>23</sup> Both photoswitchable chromophores that are toggled between emissive and nonemissive states,<sup>24,25</sup> and dynamic long-wavelength recovery of transient fluorophore dark states with frequency domain recovery<sup>26</sup> suppress background to yield up to 100-fold sensitivity improvements. Unfortunately, high-contrast photoswitchable fluorescent proteins typically require both excitations to be higher energy than that of the collected emission,<sup>27,28</sup> resulting in background and signal being similarly modulated and limiting demodulation-based discrimination. In contrast to photoswitch-based optical lock-in detection<sup>24</sup> and frequency domain photoswitching using nanoparticles,<sup>25</sup> our approach of coillumination at low energy reduces phototoxicity without generating additional background fluorescence.<sup>23,26,29,30</sup> Further, as transient dark states are optically depopulated to recover emission, molecular fluorescence is synchronized to the intensity-modulated long-wavelength

Received: May 31, 2013

Published: October 7, 2013

secondary laser, thereby directly encoding the modulation waveform only on the fluorescence signal of interest, but not on the background. Because the secondary laser excitation alters the relative population between the emissive and dark states, the magnitude of the fluorescence intensity increase is directly dependent on the rates in and out of the dark state manifold. Thus, optimization of the BFP chromophore environment for long-wavelength dark state absorption suggests using dark state lifetime as a new dimension in fluorescence imaging for fluorophore discrimination and background removal.

In developing new applications, a wide variety of optically induced spectral shifts have been optimized through fluorescent protein mutation. Essentially all switchable emitters to date, however, transiently photobleach the fluorescence-generating absorption with either thermal or very high energy (relative to collected emission) excitation-based fluorescence recovery.<sup>31,32</sup> As BFPs already optimize the blue fluorescent chromophore for emission upon near UV excitation, photoswitchable BFPs are impractical. This makes BFPs ideal candidates to optimize long-wavelength (e.g., green or yellow) recovery of blue fluorescence through dark state engineering. In contrast to photoswitches, modulatable fluorophores optically populate a low energy-absorbing, kinetically trapped dark ground state. Depending on the rates in and out of this dark state, lower energy coillumination can depopulate the dark state faster than its natural decay rate to more rapidly regenerate fluorescence, thereby altering the steady state fluorescence intensity. Mutations designed to alter chromophore protonation state in the cis vs trans chromophore configurations would likely also modify dark state lifetimes with spectrally shifted absorptions, thereby facilitating optical modulation.

## RESULTS

Optimized for brightness ( $\Phi_F = 0.45$ ) and photostability, blue emitting mKalama1 was generated from EGFP through 22 mutations that collectively stabilize the neutral form of the chromophore.<sup>18</sup> Thus, while exciting mKalama1 at 405 nm yields bright emission centered around 450 nm, coexcitation at wavelengths between 488 and 514 nm does not further increase fluorescence—it is unmodulatable. As modulation results from significant steady-state dark state population buildup, any photoaccessed mKalama1 dark states either do not absorb at 488–514 nm or are too inefficiently populated to yield measurable fluorescence enhancements.

Analogous to unmodulatable EGFP,<sup>30</sup> mKalama1 brightness appears to result from minimizing emission-degrading dark state residence. Therefore, a variant containing only the mutations essential to stabilizing the neutral chromophore was investigated. Initially formed as a double variant of wt-GFP, the mutations T203V and S205V block the green fluorescence-producing excited state proton transfer (ESPT) channels<sup>33,34</sup> between the chromophore and E222.<sup>22,35</sup> This double mutation also provides the essential element in mKalama1: stabilization of the neutral chromophore in the ground and excited states to yield a single 390 nm absorption band and 450 nm emission. Without the supporting mutations of mKalama1, this double mutation alone exhibits a lower fluorescence quantum yield of 0.29.<sup>22</sup> This less efficient fluorescence suggests that dark state population may be more likely, possibly leading to improved modulation efficiency. In addition to the base T203V/S205V, a blue fluorescent protein with additional stabilizing mutations F99S/M153T/V163A was utilized (a gift from S. J. Remington, here referred to as modBFP).<sup>22</sup> These additional mutations

partially increased the fluorescence quantum yield relative to that of modBFP (Table 1). Like mKalama1, 405 nm excitation

**Table 1. Spectroscopic Properties of Select Blue-Fluorescent Proteins**

fluorescent protein	$\lambda_{\text{abs}}/\lambda_{\text{em}}$ (nm)	quantum yield ( $\Phi_F$ )	extinction coeff ( $M^{-1} \text{ cm}^{-1}$ )	brightness <sup>b</sup>	pK <sub>a</sub>
mKalama1	385/456	0.45 <sup>a</sup>	36,000 <sup>a</sup>	16 <sup>a</sup>	5.5 <sup>a</sup>
modBFP	390/455	0.33	27,000	8.9	5.5
H148K	390/455	0.17	25,000	4.3	5.7

<sup>a</sup>Reported by Ai et al.<sup>18</sup> and used as a photophysical reference.  
<sup>b</sup>Product of  $\Phi_F$  and  $\epsilon$  in  $\text{mM}^{-1} \text{ cm}^{-1}$ .

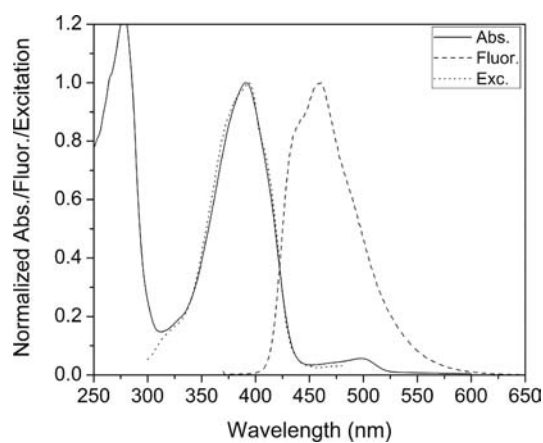


**Figure 1.** Absorption, excitation, and fluorescence spectra of modBFP.

of modBFP yields bright 450 nm emission (Figure 1), but unlike mKalama1, coexcitation of modBFP at 514 nm yields a 4% increase in fluorescence over primary excitation alone. As modulation results from populating and depopulating specific molecular energy levels, the frequency dependence of the modulation depth reports on characteristic dark state lifetimes—the characteristic time scales necessary to establish new steady-state populations under single or dual excitation conditions.<sup>30,36</sup> Analogous to frequency domain fluorescence lifetime measurements,<sup>37</sup> modulation at frequencies comparable to or faster than this inverse characteristic time scale is too fast for the molecule to respond, decreasing modulation depth. Thus, plotting modulation depth vs modulation frequency maps out the characteristic frequencies of the modulatable dark state. ModBFP exhibits a characteristic frequency of  $\sim 16$  Hz, suggesting a  $\sim 60$  ms characteristic time to establish steady-state dark state populations. Whether dominated by the rate into or out of the dark state, this long-lived state suggests the involvement of photoinduced cis–trans isomerization coupled with chromophore deprotonation giving rise to long-wavelength dark state absorption. Taking into account the very small difference between the absorption maxima of cis and trans anionic chromophores,<sup>38</sup> the 514 nm secondary laser would better match the absorption spectrum of the latter. Although other dark ground states are possible, including charge-transfer or triplet states,<sup>39,40</sup> the formation of such states is largely inconsistent with our observed long dark state lifetimes.

Informed by the published S205V crystal structure,<sup>22</sup> modifying key amino acid residues that hydrogen bond to

the tyrosine hydroxyl group in either the cis or trans chromophore form should alter modulation depth and frequency. Further, mutations that may inhibit photoisomerization are also likely to affect fluorescent manifold and dark state populations. In the more stable cis form of the chromophore, the tyrosine hydroxyl group appears to hydrogen-bond with the nitrogen atoms of H148. Position H148 in modBFP was mutated to each of the 20 amino acids to alter the excited state stability of the cis chromophore, with the goal of increasing modulation depth. While all variants exhibit a 390 nm absorbance maximum (Figure S2, Supporting Information), dual laser fluorescence enhancement was greatly affected by these mutations. Ranging between 2% and 15%, the single variants of modBFP, namely, H148G, V150A, and H148K, each further increased fluorescence enhancement under 514 nm coillumination over that of modBFP. Also noticeable is the decrease in fluorescence quantum yield of the H148K mutant (Table 1). This suggests that either a smaller residue or a more flexible side chain may favor the kinetically trapped trans isomer, possibly through larger conformational flexibility or removing a H-bond that stabilizes the cis isomer.

Fluorescence enhancement arises from secondary laser-induced recovery of the large, photoinduced steady-state dark state population generated by single laser excitation alone. Thus, the characteristic frequency is the sum of the intensity-dependent rate constant out of the bright manifold and the natural rate constant of dark state decay,  $k_{\text{bright}} + k_{\text{decay}}$ .<sup>30</sup> Modulating the secondary laser intensity dynamically increases and decreases dark state population, thereby modulating collected fluorescence. As the modulation frequency eclipses the sum of the inverse of dark state population and decay rate constants (for given primary and secondary laser excitation intensities), steady-state populations cannot be fully established during each half-modulation cycle. Thus, the modulation depth vs frequency curve reveals characteristic times corresponding to the inverse sum of rate constants into and out of the dark state, and is well-fit by phase-resolved lifetime equations (Figure 2A, eq 1, Data Analysis).<sup>37</sup>

As  $k_{\text{bright}}$  is the product of excitation rate,  $k_{\text{exc}}$  and dark state quantum yield,  $\Phi_{\text{dark}}$ ,  $k_{\text{bright}}$  generally increases with primary laser intensity. Consequently, increased primary excitation should simultaneously increase modulation depth and characteristic modulation frequency, as observed for other modulatable species. Plotting characteristic frequency vs primary intensity should yield a line that, extrapolated to zero primary intensity, yields  $k_{\text{decay}}$  as the  $y$ -intercept. The inverse of this rate constant gives the natural dark state decay time,  $\tau_{\text{decay}}$ . When coupled with the measured characteristic frequency, the average time spent in the fluorescent manifold ( $\tau_{\text{bright}} = k_{\text{bright}}^{-1}$ ) can also be determined. With these parameters, the dark state decay due to secondary illumination,  $\tau_{\text{decay},2}$  can be calculated. The characteristic times for a given set of excitation conditions are given in Table 2. As the primary intensity decreases, the characteristic frequencies of both modBFP and modBFP/H148K decrease (Figure 2B). The low primary intensity  $k_{\text{decay}}$ 's of both variants are very similar at  $\sim 6$  Hz. Different photophysics are clear in the  $\tau_{\text{bright}}$  at 560 W/cm<sup>2</sup> with modBFP being  $\sim 100$  ms and modBFP/H148K being  $\sim 30$  ms indicating more efficient photoinduced dark state formation in H148K compared to that in modBFP. As enhancement is dictated by the ratio of the single and dual laser-illuminated off and on times, the extracted photophysical times result in improved enhancement due to the H148K mutation (Table 2).

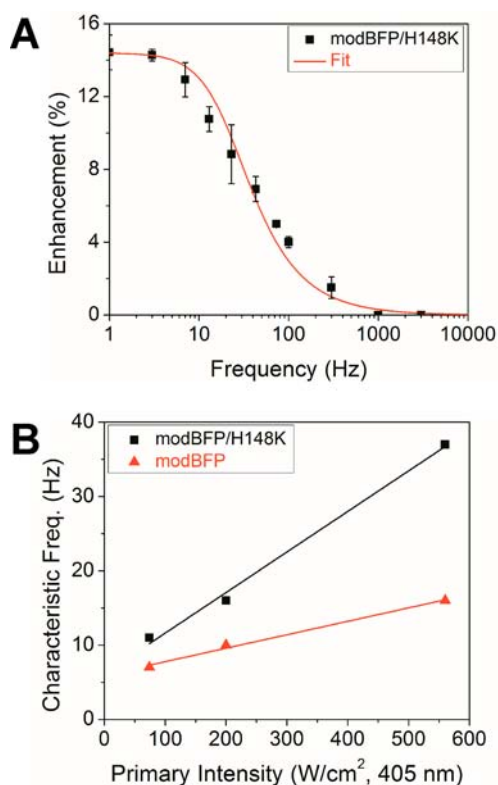


**Figure 2.** (A) Enhancement as a function of modulation frequency fitted to phase-resolved lifetime equations. (B) Characteristic frequencies are plotted as a function of 405 nm primary excitation for modBFP and modBFP/H148K. The  $y$ -intercept yields the natural dark state decay rate  $k_{\text{decay}}$  of each protein.

Less well-behaved than the modulation frequency dependence at constant excitation intensities, increasing primary intensity *decreases* total enhancement for all emitters studied (Figure 3). As fluorescence enhancement is defined as fluorescence with two lasers divided by fluorescence with primary excitation only, any dark state absorption at the primary wavelength will reduce steady-state dark state population, resulting in decreased secondary laser-induced enhancement.<sup>26</sup> Thus, a balance between populating the dark state without increasing its rate of decay must be reached, resulting in maximum enhancement being observed for both modBFP and modBFP/H148K at relatively low  $\sim 70$  W/cm<sup>2</sup> primary excitation intensity.

Analogous to studies with heavy atom-substituted xanthene dyes,<sup>26</sup> pulsed primary excitation offers the opportunity to increase  $k_{\text{bright}}$  and therefore dark state population, without increasing dark state decay,  $k_{\text{decay}}$ . Using  $\sim 90$  ps fwhm pulses at 372 nm, primary excitation only populates dark states within a short time window, allowing the modulated continuous wave (CW) secondary laser to depopulate the dark state over longer periods, without primary laser-induced dark state absorption. Thus, switching from CW 405 nm to pulsed 372 nm primary excitation, each with secondary illumination at 514 nm, increases enhancement to 20% for modBFP and 40% for modBFP/H148K using similar primary intensities (Figure 3). As long as primary-induced dark state creation is more efficient than dark state decay, such pulsed excitation prepares the dark state with a single pulse, allowing the secondary laser to optically regenerate the emissive manifold.

Table 2. Photophysical Parameters of modBFP Variants

FP	enhancement (372, 405 nm)	$\nu_c$ (Hz)	$\tau_{\text{bright}}$ (ms)	$\tau_{\text{decay}}$ (ms)	$\tau_{\text{decay},2}$ (ms)
modBFP	20%, 4%	16	100 ( $\pm 5$ )	167 ( $\pm 14$ )	157 ( $\pm 13$ )
H148D	15%, 4%	24	66 ( $\pm 5$ )	113 ( $\pm 16$ )	106 ( $\pm 15$ )
H148G	11%, 6%	30	57 ( $\pm 2$ )	222 ( $\pm 28$ )	206 ( $\pm 26$ )
H148K	37%, 15%	37	32 ( $\pm 2$ )	162 ( $\pm 35$ )	137 ( $\pm 30$ )
H148R	15%, 3%	5 <sup>a</sup>			
H148Y	5%, 2%	6 <sup>a</sup>			
V150A	20%, 10%	31	40 ( $\pm 3$ )	164 ( $\pm 56$ )	145 ( $\pm 50$ )
F165H	5%, 2%	10 <sup>a</sup>			
F165L	0	N/A			

<sup>a</sup>Larger uncertainty due to low fluorescence enhancement. Due to the poor spatial mode of the 372 nm (pulsed), on and off times were only determined for 405 nm (CW) enhancement.

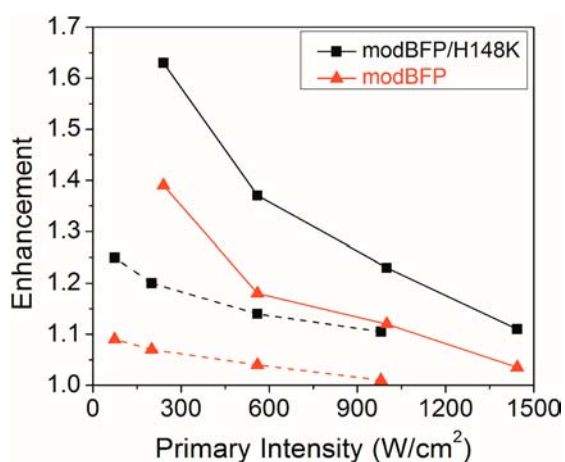


**Figure 3.** Enhancement factor versus primary intensity of pulsed 372 nm (solid) and CW 405 nm (dashed) excitation of modBFP and modBFP/H148K. Enhancement factor of 1.0 indicates no fluorescence increase over primary alone.

Mutations in close proximity to the chromophore alter not only the fluorescent species but also the energy landscape, thereby affecting stabilities of and interconversion between fluorescent and nonfluorescent populations.<sup>35,41,42</sup> The low characteristic modulation frequencies observed for all modBFP variants, coupled with the importance of the additional H148K mutation, indicate a role for cis/trans photoisomerization being at least partially responsible for modulation, perhaps coupled with differential stabilization of a long wavelength-absorbing trans isomer through hydrogen bonding to the chromophore. The marked improvement of modulation depth in modBFP/H148K suggests that mutation of the corresponding residue in mKalamal (position 149) may similarly confer modulatability upon the unmodulatable parent protein. Both mutations G149H and G149K were made, and while they display similar absorbance and emission maxima to mKalamal (Figure S3, Supporting Information), only the G149K mutation resulted in fluorescence enhancement (6%) upon coexcitation with 514 nm. Plotting the G149K fluorescence enhancement vs modulation frequency reveals a characteristic frequency of  $\sim 90$  Hz, again consistent with  $\sim 10$  ms cis–trans interconversion time scales in other fluorescent proteins.<sup>43</sup>

To demonstrate the utility of modulatable blue fluorescent proteins, we investigated selective recovery of modBFP/H148K fluorescence in the presence of a nonmodulatable background, distinguishing its emission from that of autofluorescence present in cellular imaging. NIH-3T3 cells were transfected

with a plasmid encoding modBFP/H148K fused to a mitochondrial targeting peptide (modBFP/H148K-mito). Wide field epifluorescence imaging and modulation were performed with overlapped, defocused primary (405 nm) and a smaller secondary laser excitation (514 nm). Kept somewhat smaller to maintain  $\text{kW}/\text{cm}^2$  intensities necessary for modulation, secondary excitation was modulated at 2 Hz, and emission imaged with at least 5-fold faster CCD detection. The resulting average image displays both modBFP/H148K-mito emission and autofluorescence (Figure 4). Demodulation at 2

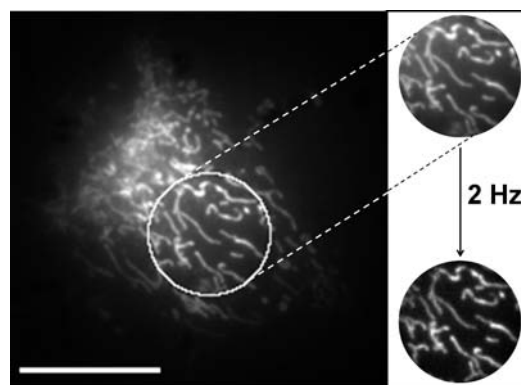


**Figure 4.** Live cell demodulation of mitochondria-targeted modBFP/H148K. Upon 405 nm illumination, autofluorescent background and blue modBFP/H148K-mito emission are collected. Coillumination at 514.5 nm, modulated at 2 Hz (secondary illumination only within the white circle), recovers only the modBFP/H148K-mito signal on a greatly reduced background (lower circle). Scale bar is 20  $\mu\text{m}$ .

Hz directly yields images with an average 5-fold improvement in signal to background as (unmodulated) autofluorescent background is removed. Signal visibility gains are further improved when raw fluorescence contrast is lower.

## DISCUSSION

Altering fluorescence enhancement stems from tuning interactions between the chromophore and the surrounding amino acid residues. As balanced rates in and out of the dark state are crucial for modulation, we can hypothesize about possible states conferring modulatability. While  $k_{\text{bright}}$  is the product of excitation rate and dark state quantum yield,  $k_{\text{decay}}$  is the natural decay out of the dark state and is associated with an energy barrier for back reversion to the fluorescent manifold (Figure 5). Consistent with our observed long dark state lifetimes and known roles of photoisomers in FP photo-switches,<sup>44,45</sup> we hypothesize that hydrogen-bonding amino

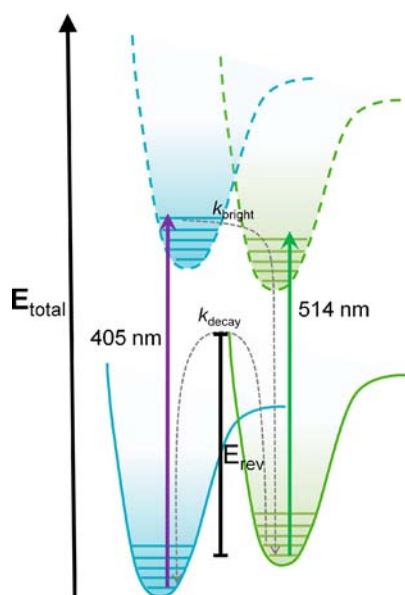


**Figure 5.** A possible schematic of energy levels involved in BFP modulation. Excitation of cis neutral state at 405 nm forms an excited state that can produce what we hypothesize as being the anionic trans state. The natural decay out of that state is  $k_{\text{decay}}$  and can be related to the activation energy for back reversion,  $E_{\text{rev}}$ . If a molecule exists in its dark state, 514 nm excitation can regenerate the blue-absorbing, fluorescent manifold.

acids that better stabilize the anionic trans chromophore in the ground and excited states increase population and residence of this kinetically trapped, but photoreversible and thermally reversible dark state. These interactions would thereby enhance modulability. Such H-bonding and steric bulk near the chromophore are likely to raise the barrier separating cis and trans forms, increasing dark state lifetime. Coupling photoisomerization with different chromophore protonation states rationalizes the observed large red-shift of the dark state absorption relative to the ground state absorption spectrum, enabling the observed optical modulation. These considerations have guided our studies and have largely borne fruit in the creation and initial understandings of optically modulatable BFPs.

Mutations of residues near the chromophore are likely to affect the energy barrier inhibiting back reversion. Structural analyses of the mutations in position 148 of FPs indicate a protective role of this position in shielding the chromophore from bulk solvent, thereby aiding emission.<sup>46,47</sup> Examining available structures, the H148 imidazole ring may hydrogen bond with nearby water molecules, instead of hydrogen bonding with the adjacent backbone strand.<sup>48</sup> Although speculative as we base mechanistic interactions on a closely related crystal structure,<sup>22</sup> the hydroxyl group of the chromophore may end up located behind the H148, which could block solvent access. Depending on the protonation state of the side chain, a weak hydrogen bond interaction with the chromophore could become possible, as this position would be within 3 Å of the cis chromophore (Figure 6A). While this interaction would stabilize the cis conformation, the resulting interaction may also influence the back reversion energy barrier. Comparing  $\tau_{\text{bright}}$  and  $\tau_{\text{decay}}$  indicates that under primary illumination the chromophore spends slightly more time in the less-stable trans anionic configuration, due to high excitation rates and a significant barrier to ground state

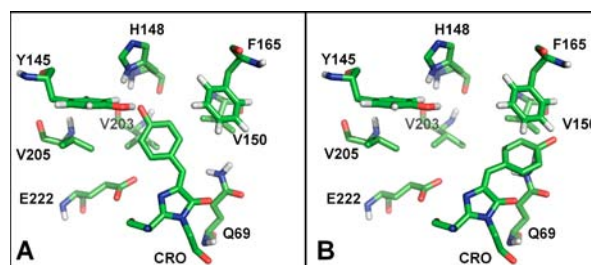


**Figure 6.** Speculative structures of the tyrosine-based chromophore in (A) cis and (B) trans positions in the chromophore pocket based on the very similar structure PDB: 2QLE.<sup>22</sup>

reversion. This steady-state dark state population is then depopulated with secondary laser illumination. Based on observed enhancements, mutations that reduce steric bulk and hydrogen bonding interactions would alter the ground state isomerization energy barrier. In contrast to the role of histidine in limiting solvent access to the chromophore, H148G mutations in GFP and YFP appear to generate a solvent channel to the chromophore cavity and increase conformational flexibility.<sup>46,48</sup> This unexpected opening of the  $\beta$ -barrel appears to reduce the hydrogen bond network around the cis chromophore and, consequently, increase the rate of photoisomerization.<sup>46</sup> This slight change may result in a stabilization of the trans state either by loosening the area around the chromophore or by providing additional hydrogen bonding partners. The result would be a decrease in trans energy, possibly increasing the reversion barrier compared to that with the histidine. In contrast, increased steric and H-bonding interactions occurring with residues such as tyrosine can destabilize the trans and decrease the reversion barrier. Interestingly, lysine would be predicted to have similar steric bulk and H-bonding capability as arginine; however, H148K has a much larger enhancement and lower  $\tau_{\text{bright}}$  values than does modBFP, suggesting an increase in the ground state energy barrier separating cis and trans. The primary amine group of lysine may interact differently with the chromophore, as the flexibility of the chain may position the amine group differently than with arginine. The difference could be reflected as an increase in energy barrier and, possibly, a change in the dark state quantum yield,  $\Phi_{\text{dark}}$ . The observed dark state lifetimes for the H148 variants are slightly longer, but of the same order of magnitude as for modBFP.

Continuing within the framework of photoisomer-coupled modulation, as mutation of the 148 residue alters the stabilization and energy barrier between the cis and trans configurations, mutation of residues near the trans configuration could have a more direct impact on the trans back reversion energy barrier. Upon 180° rotation about the central  $C_{\alpha}$ – $C_{\beta}$  bond of the chromophore, a hydrogen bond between the phenol group of the chromophore and the primary amine of the Q69 would appear likely. Investigation of the 4.0 Å area surrounding the hypothesized trans chromophore suggests that residues 150 and 165 are good candidates for mutation due to their close proximity to the chromophore (Figure 6B).<sup>22</sup> The V150A variant exhibited 10% fluorescence enhancement with a characteristic frequency of  $\sim 30$  Hz (Table 2). Though valine and alanine are both nonpolar amino acids, the methyl group of alanine is smaller than the isopropyl group of valine. As seen with H148G, a reduction in steric bulk around the trans chromophore appears to better stabilize the trans state. The

stabilization may be greater in the V150A case, as it is positioned much closer to the chromophore while in the trans position. Mutation of phenylalanine to a less bulky residue in the 165 position does not increase the observed enhancement. In fact, the 165 mutation has the opposite effect, decreasing the enhancement to 2% for histidine and eliminating it for leucine (Table 2). Though rotation to the suggested trans configuration may be less hindered in this case, the phenylalanine may have played a stabilizing role to the trans configuration by forcing the chromophore close enough to the Q69 to establish a hydrogen bond. Instead, mutation to a small, nonaromatic amino acid appears to destabilize the trans configuration, lowering the energy barrier so that the cis configuration can be more readily regenerated. This would result in faster reversion back to the fluorescent manifold, thereby decreasing both dark state lifetime and fluorescence enhancement. It should be noted that our modeling is limited in investigating all possible rotations of the chromophore, and that due to the lack of crystal structures for the bright and dark states of this exact protein variant, we can only hypothesize about the true interactions governing overall modulability. Further, rotation about another bridge and/or hula twist may lead to another type of chromophore environment. However, rotation about the central  $C_{\alpha}$ – $C_{\beta}$  of the chromophore provides a good starting point for further BFP modulation enhancement.

Most interesting is the creation of a modulatable protein from the unmodulatable mKalamal. As optimization of fluorescence quantum yield would likely minimize the energy of the back reversion, mutation would change this energy landscape reflected in fluorescence enhancement. The single mutation G149K creates a modulatable mKalama variant. This change provides an additional amino acid with a high  $pK_a$ , while simultaneously adding extra bulk near the fluorophore. This steric bulk may increase the barrier separating cis and trans chromophore forms, making the latter more thermally stable and increasing modulation efficiency.

## CONCLUSION

The utility of blue fluorescent proteins remains somewhat limited in cellular imaging due to weak fluorescence, poor photostability, and high background upon UV excitation. We propose to circumvent the sensitivity issues by developing long-wavelength optically modulated BFPs to selectively shift their signals to a unique detection frequency devoid of background. Changes to the chromophore environment directly alter the modulation depth and frequency through varied interactions that presumably differentially stabilize the neutral cis excited and anionic trans ground states. Thus, BFPs are conducive to efficient modulation, with further modulation gains possible through mutation of the chromophore environment. Changing the energy landscape to increase the efficiency of creating what appears to be a dark trans anionic state directly increases fluorescence enhancement. Most interesting is the ability to improve the fluorescence enhancement with mutations and characterize each in terms of on and off times reflecting the inverse rates into and out of the dark state. The  $\sim 100$  ms modulation time scale is postulated to involve cis/trans photoisomerization, coupled with neutral cis and anionic trans chromophore forms, or other photoreversible processes. With this guide, altering the stabilization of either state provides a route to further improving modulation of these BFPs and potentially all other color fluorescent proteins through mutagenesis.

## EXPERIMENTAL METHODS

**Protein Expression and Purification.** The gene encoding mKalamal was purchased from AddGene (Cambridge, MA). The gene was inserted between the *Xho*I and *Eco*R I restriction sites in pBAD-His B and contained an N-terminal hexahistidine tag. The plasmid was transformed into *Escherichia coli* DH5  $\alpha$ Pro. A 5 mL culture was inoculated into 1 L of LB containing 50  $\mu$ g/mL of ampicillin, grown to an OD600 of 0.5 at 37 °C (2–3 h), and then induced with 0.2% arabinose. The GFP-F99S/M153T/V163A/T203V/S205V gene was obtained as a gift from S. J. Remington (U. Oregon). The gene was inserted between *Bam*HI and *Hind*III restriction sites in PQE-30 and contained an N-terminal hexahistidine tag. The plasmid was transformed into *E. coli* M15. A 5 mL culture was inoculated into 1 L of LB containing 50  $\mu$ g/mL of ampicillin, grown to an OD600 of 0.5 at 37 °C (2–3 h), and then induced with 1 mM IPTG. Proteins were expressed to 20% of total cell protein, and protein was purified via  $Ni^{2+}$ -NTA-immobilized metal affinity chromatography (IMAC). All measurements were performed in phosphate buffer (50 mM sodium phosphate, 250 mM NaCl, pH 7.5) unless otherwise stated.

**Site-Directed Mutagenesis.** The detailed mutagenesis procedure is described in the Supporting Information.

**Construction of pAcBFP-mito Vector.** The BFP gene was amplified using gene-specific primers with additional restriction sites (*Bam*HI and *Not*I) matching the pAC-GFP-Mito1 vector (Clontech). This vector targets fluorescent proteins to the mitochondria of mammalian cells. The Ac-GFP-Mito1 vector and the amplified BFP PCR product were restricted with *Bam*HI and *Not*I in order to exchange the existing GFP in the vector for BFP. The resulting DNA products were then purified from a 1.2% agarose gel and ligated using the quick ligation kit (Epicenter) and transformed into *E. coli* DH5 $\alpha$  competent cells. The resulting Ac-BFP-Mito1 vector was verified via sequencing using BFP specific primers and then used for mammalian cell transfection.

**Protein Characterization.** Absorption and fluorescence spectra were recorded on a UV-2401 PC spectrophotometer (Shimadzu) and a PTI fluorometer (Photon Technology International), respectively. Quantum yields were measured using mKalamal as a reference.<sup>18</sup> Absorption at the excitation wavelength was kept between 0.1 and 0.5 OD. Protein concentrations were determined by comparing absorption at 280 nm to standard values based on tyrosine, tryptophan, and cysteine content. Dilutions over an order of magnitude were made for determination of chromophore extinction coefficient. For  $pK_a$  measurements, buffers were made at 10 mM buffering salt and 140 mM NaCl between pH 4 and 10.5. Proteins were diluted 30 min prior to recording enhancement data in triplicate.

**Fluorescence Microscopy.** Microscopy was performed on an inverted microscope (Olympus IX71) using a 60 $\times$  water-immersion objective (Olympus 1.2 NA). All solution data was taken by focusing 30  $\mu$ m into solution. The signal was collected in a confocal arrangement with a 100- $\mu$ m multimode fiber serving as the pinhole and directing the emission to a photon-counting avalanche photodiode (APD, Perkin-Elmer). Intensity trajectories were recorded using either a SPC-630 (Becker & Hickl) or TimeHarp 100 (Picoquant) photon counting module. Continuous wave primary excitation was used near the excitation maximum of the blue fluorescent proteins (405 nm) using a temperature controlled fiber-coupled diode laser (ThorLabs). Pulsed excitation was produced by a laser diode (Picoquant) at 372 nm and a repetition rate of 10 MHz. A line-tunable Ar<sup>+</sup> laser (Coherent) was used as secondary excitation. Appropriate band-pass filters centered near the emission wavelength of BFPs were used to efficiently block both primary and secondary laser excitation. For dual-laser excitation experiments, lasers were overlapped using a dichroic mirror prior to entering the microscope. Modulation of the secondary laser was performed with an electro-optical modulator (EOM, ConOptics, model 350-210) with square wave input. Unless otherwise stated, average primary intensities were 500 W/cm<sup>2</sup> at 405 nm and 200 W/cm<sup>2</sup> at 372 nm. Secondary intensities (514 nm) were 36 kW/cm<sup>2</sup> for both cases.

**Cell Culture.** 3T3 cells (NIH) were cultured in complete Dulbecco's modified Eagle medium (DMEM) + 10% fetal bovine serum (Atlanta Biologicals) and upon confluency, trypsinized and diluted 1:10 to reach 40% confluency after 24 h in a 6 well plate containing a glass insert for microscopy of live cells (MatTek). After 24 h, medium was changed to 1 mL of Optimem medium (Invitrogen) and the cells were transfected with 100  $\mu$ L of transfection medium containing 1  $\mu$ g of AcBFP-mito1, 3  $\mu$ L of Lipofectamine (VWR) and 93  $\mu$ L of Optimem medium per 6 wells. The transfection mixture was allowed to interact for 45 min at room temperature prior to addition to cells. After 6 h, 1 mL of complete DMEM was added to the cells followed by incubation for an additional 18 h at 37 °C, 5% CO<sub>2</sub>. After 24 h the medium was changed to complete DMEM, and cells were incubated for an additional 24 h when 48 h time points were desired.

**Cellular Imaging.** Wide field epifluorescence imaging and modulation were performed with overlapped, defocused primary and secondary laser excitation. Modulation imaging was performed by imaging (60 $\times$ , 1.2NA, Andor iXon EMCCD, 16  $\mu$ m pixels) with constant 405 nm excitation (150 W/cm<sup>2</sup>) and 514 nm laser (6 kW/cm<sup>2</sup>) modulated at 2 Hz with a camera frame rate of 12.5 Hz, typically 100 frames total. Fourier transforms of intensity versus time for each individual pixel, within the entire  $\sim$ 100-frame image stack, were calculated. Each pixel's amplitude at the modulation frequency was extracted, with these values directly yielding the demodulated image. Cells were placed on a heated stage (Biopetechs Stable "Z" Specimen Warmer) so that cells in the imaging area were held at 37 °C. Images were normalized 0 to 1, and any brightness/contrast change was done linearly and propagated to every image in the series.

**Data Analysis.** Modulated sample time traces were binned at a rate at least 2.2 times faster than the highest modulation frequency used. Fourier transformation of each time trace reveals the modulation frequency amplitude. The modulation frequency amplitude is divided by the dc amplitude and multiplied by 2 to determine the enhancement (accounting for the equal amplitude peaks at positive and negative modulation frequency). Modulation depth vs frequency curves were fit to the standard equation for frequency domain lifetime determinations:

$$m = (1 + (2\pi\nu_{\text{mod}}\tau)^2)^{-1/2} \quad (1)$$

in which  $m$  is the modulation depth,  $\nu_{\text{mod}}$  is the modulation frequency, and  $\tau$  is the characteristic lifetime. We define the characteristic frequency by the frequency at which the modulation depth drops to 50% of its original value.

## ■ ASSOCIATED CONTENT

### ● Supporting Information

Protein sequence of parent variant, absorbance and fluorescence spectra of all mutants, and additional experimental procedures. This material is available free of charge via the Internet at <http://pubs.acs.org>.

## ■ AUTHOR INFORMATION

### Corresponding Author

dickson@chemistry.gatech.edu

### Notes

The authors declare no competing financial interest.

## ■ ACKNOWLEDGMENTS

The authors thank S. J. Remington for the gift of the starting plasmid referred to as modBFP and C. J. Fahrni for the gift of starting plasmid containing the mito-targeting sequence. The authors gratefully acknowledge financial support from NIH R21EB009976 and NSF CHE-1213047.

## ■ REFERENCES

- (1) Chudakov, D. M.; Matz, M. V.; Lukyanov, S.; Lukyanov, K. A. *Physiol. Rev.* **2010**, *90*, 1103–1163.
- (2) Ormo, M.; Cubitt, A. B.; Kallio, K.; Gross, L. A.; Tsien, R. Y.; Remington, S. J. *Science* **1996**, *273*, 1392–1395.
- (3) Tsien, R. Y. *Annu. Rev. Biochem.* **1998**, *67*, 509–544.
- (4) Zimmer, M. *Chem. Rev.* **2002**, *102*, 759–781.
- (5) Shaner, N. C.; Steinbach, P. A.; Tsien, R. Y. *Nat. Methods* **2005**, *2*, 905–909.
- (6) Shaner, N. C.; Patterson, G. H.; Davidson, M. W. *J. Cell Sci.* **2007**, *120*, 4247–4260.
- (7) Lippincott-Schwartz, J.; Snapp, E.; Kenworthy, A. *Nat. Rev. Mol. Cell Biol.* **2001**, *2*, 444–456.
- (8) Lippincott-Schwartz, J.; Patterson, G. H. *Science* **2003**, *300*, 87–91.
- (9) Giepmans, B. N.; Adams, S. R.; Ellisman, M. H.; Tsien, R. Y. *Science* **2006**, *312*, 217–224.
- (10) Patterson, G. H.; Knobel, S. M.; Sharif, W. D.; Kain, S. R.; Piston, D. W. *Biophys. J.* **1997**, *73*, 2782–2790.
- (11) Remington, S. J. *Curr. Opin. Struct. Biol.* **2006**, *16*, 714–721.
- (12) Pakhomov, A. A.; Martynov, V. I. *Chem. Biol.* **2008**, *15*, 755–764.
- (13) Palm, G. J.; Zdanov, A.; Gaitanaris, G. A.; Stauber, R.; Pavlakis, G. N.; Wlodawer, A. *Nat. Struct. Biol.* **1997**, *4*, 361–365.
- (14) Patterson, G.; Day, R. N.; Piston, D. *J. Cell Sci.* **2001**, *114*, 837–838.
- (15) Subach, F. V.; Verkhusha, V. V. *Chem. Rev.* **2012**, *112*, 4308–4327.
- (16) Miyawaki, A.; Shcherbakova, D. M.; Verkhusha, V. V. *Curr. Opin. Struct. Biol.* **2012**, *22*, 679–688.
- (17) Shcherbakova, D. M.; Subach, O. M.; Verkhusha, V. V. *Angew. Chem., Int. Ed.* **2012**, *51*, 10724–10738.
- (18) Ai, H.-W.; Shaner, N. C.; Cheng, Z.; Tsien, R. Y.; Campbell, R. E. *Biochemistry* **2007**, *46*, 5904–5910.
- (19) Day, R. N.; Schaufele, F. *J. Biomed. Opt.* **2008**, *13*, 031202-031201–031202-031206.
- (20) Mena, M. A.; Treynor, T. P.; Mayo, S. L.; Daugherty, P. S. *Nat. Biotechnol.* **2006**, *24*, 1569–1571.
- (21) Kremers, G.-J.; Goedhart, J.; van den Heuvel, D. J.; Gerritsen, H. C.; Gadella, T. W. J., Jr. *Biochemistry* **2007**, *46*, 3775–3783.
- (22) Shu, X.; Leiderman, P.; Gepshtein, R.; Smith, N. R.; Kallio, K.; Huppert, D.; Remington, S. J. *Protein Sci.* **2007**, *16*, 2703–2710.
- (23) Richards, C. I.; Hsiang, J. C.; Senapati, D.; Patel, S.; Yu, J. H.; Vosch, T.; Dickson, R. M. *J. Am. Chem. Soc.* **2009**, *131*, 4619–4621.
- (24) Marriott, G.; Mao, S.; Sakata, T.; Ran, J.; Jackson, D. K.; Petchprayoon, C.; Gomez, T. J.; Warp, E.; Tulyathan, O.; Aaron, H. L.; Isacoff, E. Y.; Yan, Y. L. *Proc. Natl. Acad. Sci. U.S.A.* **2008**, *105*, 17789–17794.
- (25) Li, A. D. Q.; Zhan, C.; Hu, D. H.; Wan, W.; Yao, J. *J. Am. Chem. Soc.* **2011**, *133*, 7628–7631.
- (26) Richards, C. I.; Hsiang, J. C.; Dickson, R. M. *J. Phys. Chem. B* **2010**, *114*, 660–665.
- (27) Habuchi, S.; Ando, R.; Dedecker, P.; Verheijen, W.; Mizuno, H.; Hofkens, J. *Proc. Natl. Acad. Sci. U.S.A.* **2005**, *102*, 9511–9516.
- (28) Subach, F. V.; Zhang, L.; Gadella, T. W. J.; Gurskaya, N. G.; Lukyanov, K. A.; Verkhusha, V. V. *Chem. Biol.* **2010**, *17*, 745–755.
- (29) Vosch, T.; Antoku, Y.; Hsiang, J.-C.; Richards, C. I.; Gonzalez, J. I.; Dickson, R. M. *Proc. Natl. Acad. Sci. U.S.A.* **2007**, *104*, 12616–12621.
- (30) Jablonski, A.; Hsiang, J.; Bagchi, P.; Hull, N.; Richards, C. I.; Fahrni, C. J.; Dickson, R. M. *J. Phys. Chem. Lett.* **2012**, *3*, 3585–3591.
- (31) Rust, M. J.; Bates, M.; Zhuang, X. W. *Nat. Methods* **2006**, *3*, 793–795.
- (32) Betzig, E.; Patterson, G. H.; Sougrat, R.; Lindwasser, O. W.; Olenych, S.; Bonifacino, J. S.; Davidson, M. W.; Lippincott-Schwartz, J.; Hess, H. F. *Science* **2006**, *313*, 1642–1645.
- (33) Agmon, N. *Biophys. J.* **2005**, *88*, 2452–2461.
- (34) Agmon, N. *J. Phys. Chem. B* **2007**, *111*, 7870–7878.

- (35) Chattoraj, M.; King, B. A.; Bublitz, G. U.; Boxer, S. G. *Proc. Natl. Acad. Sci. U.S.A.* **1996**, *93*, 8362–8367.
- (36) Fan, C.; Hsiang, J.-C.; Dickson, R. M. *ChemPhysChem* **2012**, *13*, 1023–1029.
- (37) Spencer, R.; Weber, G. *Ann. N.Y. Acad. Sci.* **1969**, *158*, 361.
- (38) Addison, K.; Conyard, J.; Dixon, T.; Bulman Page, P. C.; Solntsev, K. M.; Meech, S. R. *J. Phys. Chem. Lett.* **2012**, *3*, 2298–2302.
- (39) Solntsev, K. M.; Poizat, O.; Dong, J.; Rehault, J.; Lou, Y. B.; Burda, C.; Tolbert, L. M. *J. Phys. Chem. B* **2008**, *112*, 2700–2711.
- (40) Bravaya, K. B.; Grigorenko, B. L.; Nemukhin, A. V.; Krylov, A. I. *Acc. Chem. Res.* **2012**, *45*, 265–275.
- (41) Brejc, K.; Sixma, T. K.; Kitts, P. A.; Kain, S. R.; Tsien, R. Y.; Ormo, M.; Remington, S. J. *Proc. Natl. Acad. Sci. U.S.A.* **1997**, *94*, 2306–2311.
- (42) Heim, R.; Prasher, D. C.; Tsien, R. Y. *Proc. Natl. Acad. Sci. U.S.A.* **1994**, *91*, 12501–12504.
- (43) Quercioli, V.; Bosisio, C.; Daglio, S. C.; Rocca, F.; D'Alfonso, L.; Collini, M.; Baldini, G.; Chirico, G.; Bettati, S.; Raboni, S.; Campanini, B. *J. Phys. Chem. B* **2010**, *114*, 4664–4677.
- (44) Andersen, M.; Stiel, A. C.; Trowitzsch, S.; Weber, G.; Eggeling, C.; Wahl, M. C.; Hell, S. W.; Jakobs, S. *Proc. Natl. Acad. Sci. U.S.A.* **2007**, *104*, 13005–13009.
- (45) Pletnev, S.; Subach, F. V.; Dauter, Z.; Wlodawer, A.; Verkhusha, V. V. *J. Mol. Biol.* **2012**, *417*, 144–151.
- (46) Seifert, M. H. J.; Georgescu, J.; Ksiazek, D.; Smialowski, P.; Rehm, T.; Steipe, B.; Holak, T. A. *Biochemistry* **2003**, *42*, 2500–2512.
- (47) Yang, F.; Moss, L. G.; Phillips, G. N. *Nat. Biotechnol.* **1996**, *14*, 1246–1251.
- (48) Wachter, R. M.; Elsliger, M. A.; Kallio, K.; Hanson, G. T.; Remington, S. J. *Structure* **1998**, *6*, 1267–1277.